IEEE Access
Multidisciplinary | Rapid Review | Open Access Journal

Received April 19, 2022, accepted May 9, 2022, date of publication May 12, 2022, date of current version May 19, 2022.

Digital Object Identifier 10.1109/ACCESS.2022.3174550

Nonstationary Clutter Suppression Based on Four Dimensional Clutter Spectrum for Airborne Radar With Conformal Array

YUANYI XIONG[1,2], WENCHONG XIE[2], (Member, IEEE), AND YONGLIANG WANG[1,2]
[1]College of Electronic Science and Technology, National University of Defense Technology, Changsha 410073, China
[2]Wuhan Radar Academy, Wuhan 430019, China

Corresponding author: Wenchong Xie (xwch1978@163.com)

This work was supported in part by the National Science and Technology Excellence Youth Science Foundation of China under Grant 2019-JCJQ-ZQ-006.

ABSTRACT Conformal array antenna is one of the important development directions of airborne radar in the future. Its advantages include aerodynamic design, larger effective aperture and minimal payload weight etc. However, conformal array antenna usually has non-linearity feature. The special geometry deteriorates the performance of the antenna pattern and causes nonstationary clutter distribution. The performance of conventional space time adaptive processing (STAP) methods is degraded. Aiming at the clutter suppression problem of the conformal array airborne radar under the situation of range ambiguity, a four-dimensional space-time clutter spectrum adaptive compensation method has been proposed. Based on the establishment of a conformal array airborne radar clutter signal model and clutter distribution characteristics, this method transforms the conformal array into a virtual uniform linear array, and estimates the four-dimensional minimum variance distortionless response (MVDR) spectra by means of space-time smoothing processing. Then it compensates the data in the short-range nonstationary clutter region, and estimates the clutter and noise covariance matrix based on the compensated data to perform space time adaptive processing. This method does not move the target signal while realizing the short-range nonstationary clutter compensation. At the same time, by compensating the data of all the short-range regions, it overcomes the influence of prior system parameter error and array error on the compensation methods, which has strong robustness feature. The simulation results verify the effectiveness of the proposed method.

INDEX TERMS Conformal array, clutter suppression, STAP, airborne radar, four-dimensional clutter spectrum.

I. INTRODUCTION

The conformal array (CFA) antenna can provide an aerodynamic shape consistent with the shape of the platform without increasing the radar cross section (RCS) of the platform or affecting its aerodynamic performance. At the same time, it can produce a relatively larger effective aperture and minimal payload weight. Therefore, the conformal array airborne radar is one of the important development directions of the airborne early warning radar in the future, especially for unmanned platforms and payload-limited platforms [1]. However, conformal array antennas usually have non-linearity feature. On the one hand, the characteristic deteriorates the performance of the antenna pattern; on the other hand, the clutter signal is nonstationary, which makes the number of training samples that meet the independent and identically distributed (I.I.D.) condition insufficient [2]–[7]. In [4] and [5], they addressed the problem of classifying clutter and clutter edge detection, it would allow us to cluster the entire region under surveillance into homogeneous sets that can be used for estimation purposes. But they cannot solve the problem of dense distribution of interference signals or the limited number of the training snapshots. So the formed space time adaptive processing (STAP) filter is inconsistent with the real echo data of the detected range cell, which leads the clutter suppression performance strongly degraded.

The conventional nonstationary clutter suppression methods for conformal array airborne radar include: (1) Localized

The associate editor coordinating the review of this manuscript and approving it for publication was Mohammad Tariqul Islam.

processing, that is, the reduced-dimension STAP methods [6]–[9]. This type of method minimizes the impact of nonstationarity by reducing the training sample requirement; (2) Time-varying weights, that is, derivative based updating method (DBU) [10]–[12]. This method assumes that there exists a linear relationship between space-time adaptive weight and range. However, the demand for the number of training samples is doubled; (3) Clutter compensation methods [13]–[21]. This type of method performs clutter compensation based on a one-dimensional or two-dimensional space-time plane. In [20], we have proposed a space-time compensation STAP method based on adaptive segmentation, but it is just suitable for the actual clutter environment faced by the bistatic airborne radar with typical configurations. The registration-based compensation (RBC) method considering range ambiguity, denoted RBC-RA, was proposed in [21], which compensates the unambiguous range cell and the ambiguous range cell to the corresponding reference range cell respectively. The nonstationary clutter compensation accuracy is high, but it has a strong dependence on the prior parameters of the airborne radar system. (4) Clutter reconstruction methods [22]–[28]. These methods perform STAP by reconstructing the clutter plus noise covariance matrix based on the priori knowledge. In [23], a knowledge-aided sparse recovery (SR) STAP algorithm based on Gaussian kernel function is proposed, they use the prior knowledge that the clutter components are distributed along the clutter ridge, but when it exists prior parameter error or array error, the clutter ridge cannot be calculated precisely. In [25], the Bayesian estimate for the covariance matrix is associated with the prior covariance estimate and maximum likelihood (ML) covariance estimate. However, when the prior covariance has errors, the performance of the clutter reconstruction method is limited.

In this paper, a nonstationary clutter suppression method based on four dimensional clutter spectrum for conformal array airborne radar is proposed. This method transforms the conformal array into a virtual uniform linear array, and then estimates the four-dimensional minimum variance distortionless response (MVDR) spectra through space-time smoothing processing. The clutter data in the short-range nonstationary clutter region is compensated according to the farthest unambiguous reference range cell. Finally, it estimates the clutter and noise covariance matrix based on the compensated data to perform STAP. The simulated results show that the proposed method achieves a significant performance for STAP and overcomes the influence of prior system parameter error and array error on compensation processing.

The remainder of this paper is organized as follows. The clutter signal model of conformal array airborne radar is established in Section II, which takes the range ambiguity into account. Section III analyzes the clutter distribution characteristics, including clutter trajectory, clutter power spectrum and clutter range-Doppler spectrum of conformal array. Section IV provides the specific details of the four-dimensional space-time clutter spectrum adaptive compensation method. Section V quantifies performance potential of the proposed method by means of the simulation results. Finally, the conclusions are provided in Section VI.

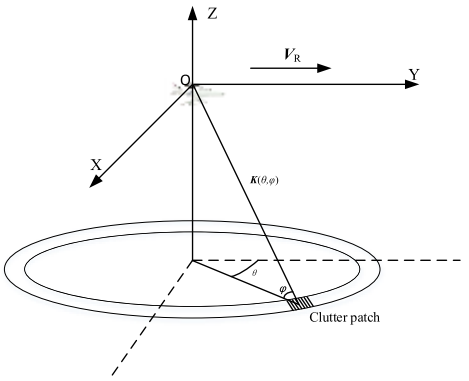

FIGURE 1. Airborne radar geometry.

II. SIGNAL MODELS

The airborne radar geometry is shown in Fig. 1. The coordinate system (X, Y, Z) represents the platform coordinate system. The platform moves in the positive direction along the Y axis. For a sidelooking array, it is placed along the Y axis, and for a forward-looking array, it is placed along the X axis. As for Fig. 1, the position of a clutter patch at a certain range cell is expressed as (θ, φ), θ is the azimuth angle of the clutter patch, and φ is the pitch angle. The radar antenna beam direction corresponding to the clutter patch is defined as $\boldsymbol{K}(\theta, \varphi) = [\sin\theta\cos\varphi, \cos\theta\cos\varphi, -\sin\varphi]^{\mathrm{T}}$, The motion vector of the radar platform is defined as $\boldsymbol{V}_{\mathrm{R}} = V_{\mathrm{R}}[0,1,0]^{\mathrm{T}}$. The spatial position coordinate of the mth antenna element is (x_m, y_m, z_m), m=1,2,...,M, M is the total number of element.

Different from the planar phased array antenna, the element gain of the conformal array antenna is related to the placement direction of the element, so the element gain of the mth element is

$$g_{e/m}(\beta_m) = \begin{cases} g_0 \cos^2(\beta_m \dfrac{\pi}{\theta_{\mathrm{null}}}), & -\dfrac{\pi}{2} \le \beta_m \le \dfrac{\pi}{2} \\ g_b g_0 \cos^2(\beta_m \dfrac{\pi}{\theta_{\mathrm{null}}}), & \dfrac{\pi}{2} < \beta_m < \dfrac{3\pi}{2} \end{cases} \quad (1)$$

where g_0 is the peak gain of the array element, $g_b$is the backward attenuation coefficient, θ_{null} is the zero-zero mainlobe width of the array element pattern, β_m is the angle between the direction of the radar beam corresponding to the clutter patch and the surface normal vector $\boldsymbol{n}_{e/m}$ to the mth element, and

$$\beta_m = \cos^{-1}(\boldsymbol{n}_{e/m} \cdot \boldsymbol{K}(\theta, \varphi)) \quad (2)$$

Assuming that M elements are synthesized into a subarray, the pattern of the subarray is

$$F(\theta, \varphi) = \sum_{m=1}^{M} \mathrm{e}^{\mathrm{j}\frac{2\pi}{\lambda}[\boldsymbol{K}(\theta,\varphi)-\boldsymbol{K}(\theta_0,\varphi_0)]\cdot\boldsymbol{d}_{e/m}} \cdot F_{e/m}(\theta) \quad (3)$$

where $F_{e/m}(\theta)$ is the amplitude pattern of the mth element, $\boldsymbol{d}_{e/m}$ is the direction vector to the mth element, and its corresponding antenna gain is

$$G(\theta, \varphi) = Mg_0 \left|\bar{F}(\theta, \varphi)\right|^2 \tag{4}$$

where $\bar{F}(\theta, \varphi)$ is the normalized pattern of the subarray. The space steering vector is

$$\boldsymbol{S}_s(f_s) = \left[e^{j2\pi \frac{\boldsymbol{K}(\theta,\varphi)\cdot\boldsymbol{d}_{e/1}}{\lambda}}, e^{j2\pi \frac{\boldsymbol{K}(\theta,\varphi)\cdot\boldsymbol{d}_{e/2}}{\lambda}}, \cdots, e^{j2\pi \frac{\boldsymbol{K}(\theta,\varphi)\cdot\boldsymbol{d}_{e/N}}{\lambda}} \right]^T \tag{5}$$

where N is the number of receive subarrays.

The time steering vector is not affected by the spatial geometry of the conformal array, and can be expressed as

$$\boldsymbol{S}_t(f_d) = \left[1, e^{j2\pi \frac{2\boldsymbol{K}(\theta,\varphi)\cdot\boldsymbol{V}_R}{\lambda f_r}}, \cdots, e^{j2\pi \frac{2\boldsymbol{K}(\theta,\varphi)\cdot\boldsymbol{V}_R}{\lambda f_r}(K-1)} \right]^T \tag{6}$$

where K is the number of coherent pulses, λ is the radar wavelength, f_r is the pulse repetition frequency (PRF). The space-time steering vector corresponding to the clutter patch in Fig. 1 is

$$\boldsymbol{S}(f_s, f_d) = \boldsymbol{S}_t(f_d) \otimes \boldsymbol{S}_s(f_s) \tag{7}$$

If both temporal sampling and spatial sampling are considered, the echo signal vector of the clutter patch is

$$\boldsymbol{X}_c(\theta_i, \varphi_l) = a_{i,l}\boldsymbol{S}(f_s, f_d) \tag{8}$$

where $a_{i,l}$ is random amplitude of the clutter signal, and $E\left\{\left|a_{i,l}\right|^2\right\} = \sigma^2 CNR_{i,l}$, σ^2 is the noise power per element,

$$CNR_{i,l} = \frac{P_t G_t(\theta_i, \varphi_l) G_r(\theta_i, \varphi_l) \lambda^2 \sigma_{i,l} D}{(4\pi)^3 R_l^4 K' T_0 B F_n L_s} \tag{9}$$

$G_t(\theta_i, \varphi_l)$ and $G_r(\theta_i, \varphi_l)$ are the transmit gain and receive subarray gain of the conformal array antenna, and the expression of $G_r(\theta_i, \varphi_l)$ is as shown in (4). P_t is the peak transmit power, $\sigma_{i,l}$ is the clutter patch reflectivity, D is the pulse compression gain, R_l is the distance from the radar to the patch, K' is Boltzman's constant, T_0 is the system temperature, B is the receiver bandwidth, F_n is the receiver noise coefficient, L_s is radar system loss.

Because the echoes of the same range cell reach the radar receiver at the same time, the clutter signal of the lth range cell is

$$\boldsymbol{X}_{cl} = \sum_{i=1}^{N_c} a_{i,l}\boldsymbol{S}(f_s, f_d) \tag{10}$$

where N_c is the number of independent clutter patches of each range cell. Considering the range ambiguity, then

$$\boldsymbol{X}_c = \sum_{l=1}^{N_r}\sum_{i=1}^{N_c} a_{i,l}\boldsymbol{S}(f_s, f_d) \tag{11}$$

where N_r is the number of range ambiguity.

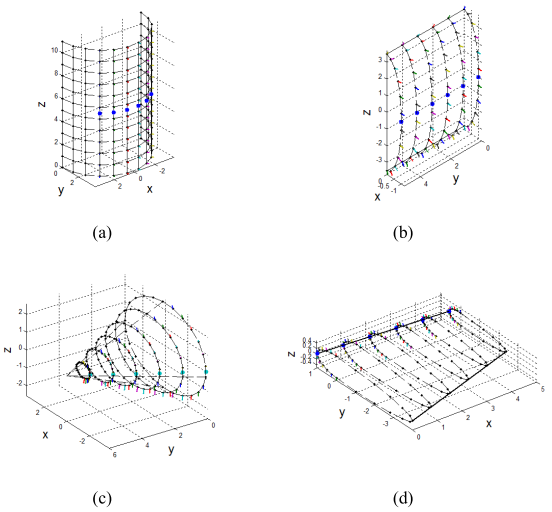

FIGURE 2. Conformal array antenna geometry. (a) Cylindrical array. (b) Fuselage array. (c) Nose cone conformal array. (d) Wing conformal array.

III. CLUTTER CHARACTERISTICS OF CONFORMAL ARRAY AIRBORNE RADAR

Considering that the receive subarray of conformal array antenna usually has nonlinear characteristics at a certain moment, it may be a linear array, a curved array [29], or even a curved plane array [10], so the spatial frequency of a one-dimensional linear array cannot meet the analysis requirements. The reason is that the one-dimensional linear array can only sense one-dimensional spatial frequency, while the curved array can sense two-dimensional spatial frequency, and the curved plane array can even sense three-dimensional spatial frequency. This section expands the spatial frequency from one dimension to three dimensions.

As shown in Fig. 1, for any clutter patch, the Doppler frequency of the echo signal can be expressed as

$$f_d = \frac{2\boldsymbol{K}(\theta, \varphi)\cdot\boldsymbol{V}_R}{\lambda} = \frac{2V_R\cos\theta\cos\varphi}{\lambda} \tag{12}$$

It is worth noticing that the Doppler frequency of the clutter patch is related to the position of the clutter patch and the flight direction of the platform, which has nothing to do with the shape of the antenna and the placement form. The normalized Doppler frequency is

$$\bar{f}_d = \frac{f_d}{f_r} = \frac{2V_R\cos\theta\cos\varphi}{\lambda f_r} \tag{13}$$

The spatial frequency corresponding to the clutter patch can be expressed as [30]

$$\boldsymbol{f}_s = \frac{\boldsymbol{K}(\theta, \varphi)}{\lambda} = \frac{[\sin\theta\cos\varphi, \cos\theta\cos\varphi, -\sin\varphi]}{\lambda} \tag{14}$$

Then the normalized spatial frequency is

$$\begin{aligned}\bar{\boldsymbol{f}}_s &= \frac{\boldsymbol{f}_s}{1/0.5\lambda} = [0.5\sin\theta\cos\varphi, 0.5\cos\theta\cos\varphi, -0.5\sin\varphi] \\ &= [f_{sx}, f_{sy}, f_{sz}]\end{aligned} \tag{15}$$

In this section, a phased array antenna containing 72 elements is taken as an example to analyze the clutter distribution characteristics of the conformal array airborne radar. The four practical conformal array antenna geometry is shown in Fig. 2. The arrow indicates the placement direction of each array element, the big dot indicates the phase center position of the receive subarray, and each coordinate is normalized by half wavelength.

The conventional sidelooking array, non-sidelooking array, and forward-looking array with same number of elements [6], [7] are compared in the subsequent analysis. Due to lack of space, the results are no longer given in this section.

A. CLUTTER TRAJECTORY

Fig. 3 shows the distribution of airborne radar clutter trajectories in the three-dimensional spatial frequency and Doppler frequency domains at a fixed range cell. The conclusions can be drawn from Fig. 3 as follows. (1) The clutter trajectory is distributed as a slanted circle in $(f_{sx}, f_{sy}, \bar{f}_d)$ domain. For the sidelooking array, it can only sense the spatial frequency along the axis of the array, that is, the Y-axis direction, so the clutter trajectory is a diagonal line on the $(f_{sy}, \bar{f}_d)$ plane, as shown in Fig. 3(a); for the forward-looking array, it can only sense the spatial frequency along the X-axis, so its clutter trajectory is a circle on the $(f_{sx}, \bar{f}_d)$ plane as shown in Fig. 3(a); for non-sidelooking array, it can sense the spatial frequencies in the X-axis and Y-axis directions at the same time. When the spatial circular trajectory shown in Fig. 3(a) is projected to the axial direction of the array where the non-sidelooking array is located, that is, the elliptical trajectory can be obtained. For the fuselage conformal array antenna, the receive subarray is a linear array along the Y-axis, so the clutter trajectory is the same as that of the sidelooking array. For the cylindrical array, the receive subarray is on the (X, Y) plane, and it can acquire the spatial frequencies of the X and Y axes simultaneously. For the nose cone and wing conformal arrays, the receive subarray is a one-dimensional linear array, and the clutter distribution trajectory is the same as the non-sidelooking array. (2) The distribution of clutter trajectories in the three-dimensional frequency domain (f_{sx}, f_{sy}, f_{sz}) is a sphere of radius 0.5, and the clutter trajectory of a certain range cell is the intersection of the (f_{sx}, f_{sy}) plane with the sphere, regardless of the array configuration.

Fig. 4 shows the variation of the airborne radar clutter trajectories with range, and the larger the ellipse, the farther the distance. The conclusions can be drawn as follows. (1) As for arbitrary antenna arrays, the clutter trajectories vary with range. The closer the range is, the more obvious the variation is. On the contrary, the farther the range is, the more gentle the variation is, and the clutter trajectories can be considered to be stationary. (2) As for the fuselage conformal array, its clutter trajectories are the same as that of the sidelooking array, and only the range of clutter trajectories varies with the distance. So the clutter of the fuselage conformal array is generally considered to be stationary.

B. CLUTTER POWER SPECTRUM

Fig. 5 shows four clutter power spectra of airborne array radar with conformal array, and they are the results of four-dimensional power spectra projected into two three-dimensional domains, the quantity represented in the colour axis means the relative power.

Fig. 6 shows the antenna pattern. The conclusions can be drawn from Fig. 5 as follows. (1) In the $(f_{sx}, f_{sy}, \bar{f}_d)$ domain, the clutter power spectrum is distributed along a tilted circle, and this conclusion is consistent with Fig. 3(a). The difference between different antenna configurations is the distribution of clutter power. (2) In the (f_{sx}, f_{sy}, f_{sz}) domain, the clutter power spectrum is distributed along a certain cross section parallelling to the (f_{sx}, f_{sy}) plane, and the conclusion is consistent with Fig. 3(b). (3) It should be noticed that for the fuselage conformal array, the clutter power spectrum shows a certain degree of particularity in the $(f_{sx}, f_{sy}, \bar{f}_d)$ domain as shown in Fig. 5(b). For the cylindrical array, the nose cone conformal array and the wing conformal array, part of the clutter is also distributed in other places of the sphere in addition to the cross-section in the (f_{sx}, f_{sy}, f_{sz}) domain. The reason is due to the array antenna pattern as shown in Fig. 6.

C. CLUTTER RANGE-DOPPLER SPECTRUM

Fig. 7 shows clutter range-Doppler spectra of four conformal arrays. It can be seen from Fig. 7 that the clutter range-Doppler spectrum of the fuselage conformal array is similar to that of the sidelooking array. The clutter range-Doppler spectrum of the cylindrical array is basically the same as the forward-looking array, but there is strong clutter at the normalized Doppler frequency 0.28. The reason is that the cylindrical array pattern has a high sidelobe level at 34°, as shown in Fig. 6(a). Therefore, the normalized Doppler frequency is

$$\bar{f}_d = \frac{2V_R \cos(90° - 34°)\cos(1°)}{\lambda f_r} = 0.28 \tag{16}$$

where the platform velocity V_R =140m/s, radar wavelength λ =0.23m, PRF f_r =2434.8Hz.

The clutter range-Doppler spectrum of the nose cone conformal array is basically the same as that of the non-sidelooking array, with its beam pointing to the 135° direction, and the corresponding normalized Doppler frequency of the mainlobe clutter is 0.35. However, there is strong clutter at the normalized Doppler frequency -0.06. The reason is that the antenna pattern of the nose cone conformal array has a high sidelobe level at 37°, as shown in Fig. 6(b). The clutter range-Doppler spectrum of the wing conformal array is similar to that of the forward-looking array, but there is strong clutter at the normalized Doppler frequency 0.2, which is due to the direction of the wing conformal array antenna corresponding to the high sidelobe level at 157°, as shown in Fig. 6(c).

Through the analysis of the clutter distribution characteristics of the conformal array airborne radar, the following conclusions can be drawn. (1) Under the premise of the

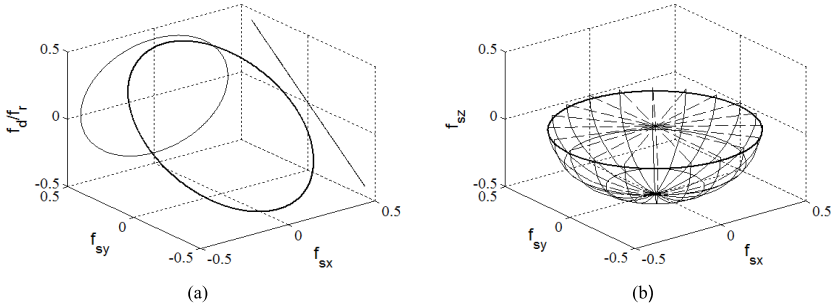

FIGURE 3. Space-time trajectory distribution of clutter. (a) $\left(f_{sx}, f_{sy}, \bar{f}_d\right)$. (b) (f_{sx}, f_{sy}, f_{sz}).

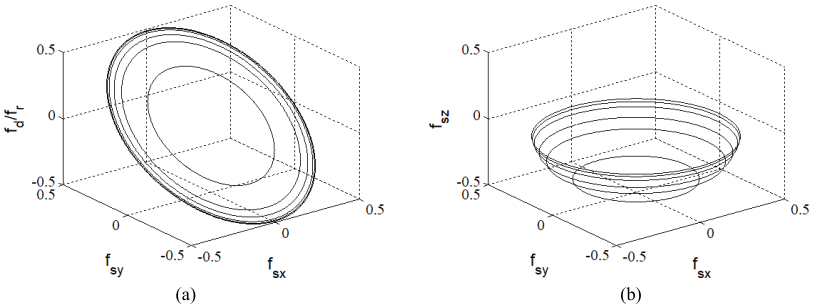

FIGURE 4. The relationship between clutter trajectory and range. (a) $\left(f_{sx}, f_{sy}, \bar{f}_d\right)$. (b) (f_{sx}, f_{sy}, f_{sz}).

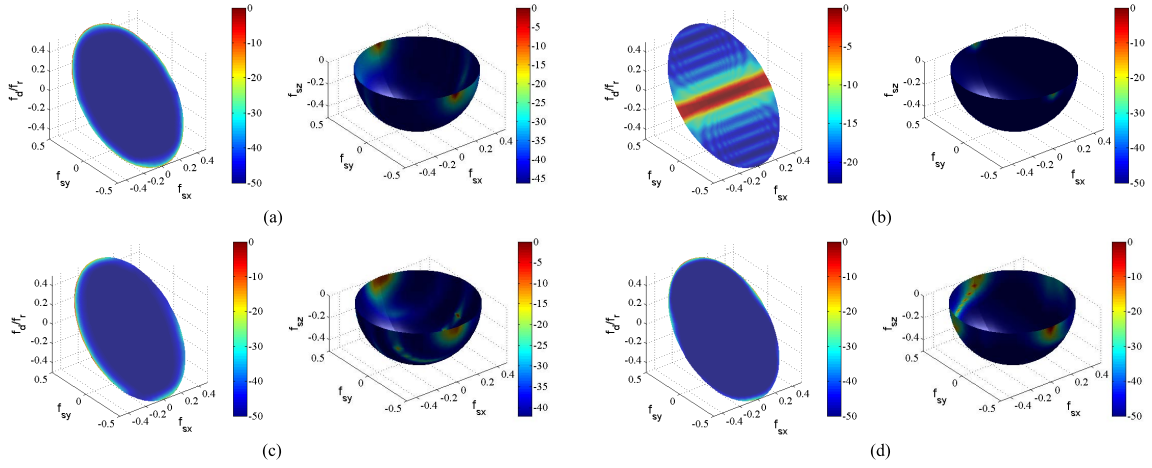

FIGURE 5. Clutter power spectra. (a) Cylindrical array. (b) Fuselage array. (c) Nose cone conformal array. (d) Wing conformal array.

coordinate system, the distribution of clutter trajectory on the space-time plane has nothing to do with the array configuration. (2) Different arrays can sense the clutter frequencies in different spatial domains. When the receive subarray is a linear array, the space-time trajectory of clutter only needs to be projected to the plane where the array axis is located to obtain the corresponding clutter distribution trajectory. When it is a curved array, the clutter trajectory needs to be characterized in multiple spatial domains simultaneously. (3) The clutter power spectrum distribution characteristics are consistent with the clutter trajectory, and the specific power distribution on the trajectory is relevant with the geometric configuration of the radar platform, antenna pattern and other factors. (4) The clutter distribution of the fuselage conformal array antenna is basically the same as that of the forward-looking array. (5) Due to the particularity of the antenna pattern for the cylindrical array, the nose cone conformal array and the wing conformal array, their clutter distribution is different from that of the planar array antenna. (6) In addition to the fuselage conformal array, the clutter spectra of the cylindrical, the nose cone conformal array and the wing conformal array show severe nonstationary distribution characteristics in the range dimension. This is the manifestation of array-induced, nonstationary clutter problem in STAP.

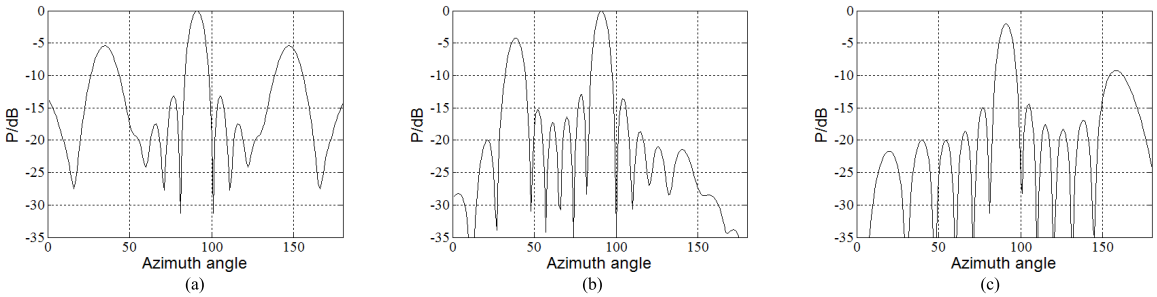

FIGURE 6. Antenna pattern of three different arrays. (a) Cylindrical array. (b) Nose cone conformal array. (c) Wing conformal array.

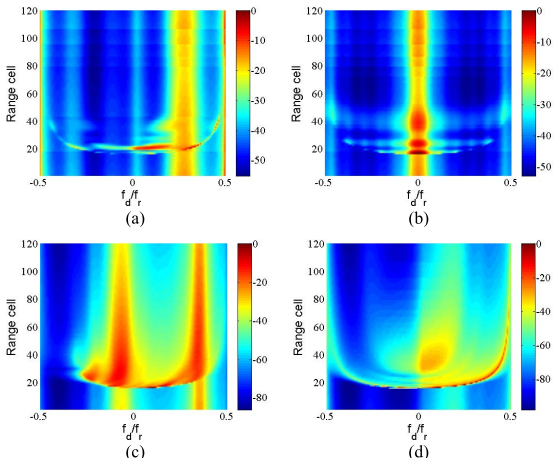

FIGURE 7. Clutter range-Doppler spectra. (a) Cylindrical array. (b) Fuselage conformal array. (c) Nose cone conformal array. (d) Wing conformal array.

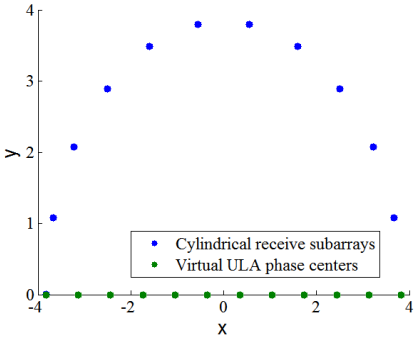

FIGURE 8. The cylindrical receive subarrays and virtual ULA phase centers.

IV. CLUTTER SUPPRESSION METHOD

The analysis of the clutter characteristics of the conformal array airborne radar in Section III shows that the clutter presents serious nonstationary characteristics in the range dimension. This section proposes a four-dimensional space-time clutter spectrum adaptive compensation method for the conformal array airborne radar, namely the 4D-STC method.

A. PROPOSED METHOD

This method first transforms the conformal array into a virtual uniform linear array. Then the echo covariance matrix of each range cell is estimated through smoothing processing, and the space-time echo data is transformed into the four-dimensional space-time power spectrum domain. The short-range nonstationary clutter is compensated to the maximum unambiguous range cell. Finally, it uses the compensated space-time data to estimate the clutter covariance matrix of the range cell to be detected, and forms the space-time adaptive weight to achieve clutter suppression.

The main steps of the proposed method are as follows.

Step 1: Virtual Uniform Linear Array Transformation:

For space smoothing processing, the premise is that the subarrays are uniformly distributed [31]. However, the conformal array receive subarrays usually cannot meet this requirement. Therefore, for the conformal array antenna, in order to facilitate subsequent space smoothing processing, this method first transforms the conformal array into a virtual uniform linear array (ULA). Fig. 8 shows the relationship between the cylindrical receive subarrays and virtual ULA phase centers, and the virtual ULA phase centers are defined so that they are perpendicular to the platform motion direction. As for other conformal arrays in Fig. 2, since the form of receive subarrays is uniform linear array, this step is not required.

Assuming that the spatial sampling signals of the lth range cell corresponding to the conformal array and the virtual uniform linear array are $\boldsymbol{X}_{l,\mathrm{s}}$ and $\tilde{\boldsymbol{X}}_{l,\mathrm{s}}$, respectively, the transformation operation [32] is

$$\tilde{\boldsymbol{X}}_{l,\mathrm{s}} = \boldsymbol{T}_l^{\mathrm{H}} \boldsymbol{X}_{l,\mathrm{s}} \tag{17}$$

where the expression of the transformation matrix $\boldsymbol{T}_l$ is

$$\boldsymbol{T}_l = \left(\boldsymbol{S}_{\mathrm{s},l,\mathrm{ULA}}(\boldsymbol{\theta})\, \boldsymbol{S}^{\dagger}_{\mathrm{s},l,\mathrm{CFA}}(\boldsymbol{\theta})\right)^{\mathrm{H}} \tag{18}$$

$$\boldsymbol{S}_{\mathrm{s},l,\mathrm{ULA}}(\boldsymbol{\theta}) = \left[\boldsymbol{S}_{\mathrm{s},l,\mathrm{ULA}}(\theta_1)\ \boldsymbol{S}_{\mathrm{s},l,\mathrm{ULA}}(\theta_2)\ \cdots\ \boldsymbol{S}_{\mathrm{s},l,\mathrm{ULA}}\left(\theta_{N_{\mathrm{a}}}\right)\right]$$

$$\boldsymbol{S}_{\mathrm{s},l,\mathrm{ULA}}\left(\theta_{i_{\mathrm{a}}}\right) = \sum_{i_{\mathrm{r}}=1}^{N_{\mathrm{r}}} \boldsymbol{S}_{\mathrm{s},l,\mathrm{ULA}}\left(\theta_{i_{\mathrm{a}}}, \varphi_{i_r}\right) \tag{19}$$

$$\boldsymbol{S}_{\mathrm{s},l,\mathrm{CFA}}(\boldsymbol{\theta}) = \left[\boldsymbol{S}_{\mathrm{s},l,\mathrm{CFA}}(\theta_1)\ \boldsymbol{S}_{\mathrm{s},l,\mathrm{CFA}}(\theta_2)\ \cdots\ \boldsymbol{S}_{\mathrm{s},l,\mathrm{CFA}}\left(\theta_{N_{\mathrm{a}}}\right)\right]$$

$$\boldsymbol{S}_{\mathrm{s},l,\mathrm{CFA}}\left(\theta_{i_{\mathrm{a}}}\right) = \sum_{i_{\mathrm{r}}=1}^{N_{\mathrm{r}}} \boldsymbol{S}_{\mathrm{s},l,\mathrm{CFA}}\left(\theta_{i_{\mathrm{a}}}, \varphi_{i_r}\right) \tag{20}$$

where $(\cdot)^{\dagger}$ represents the pseudo-inverse operation, $\boldsymbol{S}_{\mathrm{s},l,\mathrm{CFA}}(\boldsymbol{\theta})$ and $\boldsymbol{S}_{\mathrm{s},l,\mathrm{ULA}}(\boldsymbol{\theta})$ are the space steering vectors corresponding to the conformal array and the virtual uniform linear array, respectively, N_{a} is the number of constrained azimuth angles, usually $N_{\mathrm{a}} > N$, and N_{r} is the number of range ambiguities.

For any conformal array, when the curvature of the conformal surface changes gently, the virtual transformation can obtain the ideal transformation accuracy. When the curvature of the conformal surface changes steeply, the virtual transformation accuracy will deteriorate, but still in an acceptable range. Fortunately, the surface radian of fuselage, wing and nose cone conformal array changes gently in practical engineering, so the virtual transformation has its applicability.

Step 2: Four-Dimensional Space-Time Clutter Spectrum Estimation:

Suppose the space-time sampling echo signal of virtual linear array for the lth range cell is

$$\tilde{\boldsymbol{X}}_l = \begin{bmatrix} \tilde{x}_{l,00} & \tilde{x}_{l,01} & \tilde{x}_{l,02} & \cdots & \tilde{x}_{l,0(K-1)} \\ \tilde{x}_{l,10} & \tilde{x}_{l,11} & \tilde{x}_{l,12} & \cdots & \tilde{x}_{l,1(K-1)} \\ \tilde{x}_{l,20} & \tilde{x}_{l,21} & \tilde{x}_{l,22} & \cdots & \tilde{x}_{l,2(K-1)} \\ \vdots & \vdots & & \ddots & \\ \tilde{x}_{l,(N-1)0} & \tilde{x}_{l,(N-1)1} & \tilde{x}_{l,(N-1)2} & \cdots & \tilde{x}_{l,(N-1)(K-1)} \end{bmatrix} \tag{21}$$

Assuming that the size of the spatial and temporal window are N' and K' respectively, it can obtain Q samples, where $Q \geq 2N'K'$, namely

$$Q = \left(N - N' + 1\right)\left(K - K' + 1\right) \tag{22}$$

Using the Q samples $\tilde{\boldsymbol{X}}_{l,q}$, $q = 0, 1, \cdots, Q-1$ obtained by the spatial and temporal smoothing technique [31] to estimate the clutter covariance matrix of the range cell, namely

$$\hat{\boldsymbol{R}}_l^{(\mathrm{s})} = \frac{1}{Q}\sum_{q=0}^{Q-1} \tilde{\boldsymbol{X}}_{l,q}\tilde{\boldsymbol{X}}_{l,q}^{\mathrm{H}} \tag{23}$$

The four-dimensional space-time clutter spectrum corresponding to the echo of the lth range cell estimated by space-time smoothing processing is

$$\hat{\boldsymbol{P}}_l\left(f_{\mathrm{sx}}, f_{\mathrm{sy}}, f_{\mathrm{sz}}, \bar{f}_{\mathrm{d}}\right) = \frac{1}{\boldsymbol{S}^{(\mathrm{s})\mathrm{H}}(f_{\mathrm{sx}}, f_{\mathrm{sy}}, f_{\mathrm{sz}}, \bar{f}_{\mathrm{d}})\left(\hat{\boldsymbol{R}}_l^{(\mathrm{s})}\right)^{-1}\boldsymbol{S}^{(\mathrm{s})}(f_{\mathrm{sx}}, f_{\mathrm{sy}}, f_{\mathrm{sz}}, \bar{f}_{\mathrm{d}})} \tag{24}$$

where $\boldsymbol{S}^{(\mathrm{s})}(f_{\mathrm{sx}}, f_{\mathrm{sy}}, f_{\mathrm{sz}}, \bar{f}_{\mathrm{d}})$ is the subaperture space-time steering vector

The power corresponding to the virtual linear array at each point on the four-dimensional grid can be obtained from (24), and we still need to transform it into the power corresponding to the conformal array. Through the space-time frequency of each grid of the virtual linear array, the corresponding azimuth and elevation angle can be calculated, and then the power $\hat{\boldsymbol{P}}_l\left(f_{\mathrm{sx}}, f_{\mathrm{sy}}, f_{\mathrm{sz}}, \bar{f}_{\mathrm{d}}\right)$ is mapped to the power on the four-dimensional grid of the conformal array with the same azimuth and elevation angle, i.e., $\tilde{\hat{\boldsymbol{P}}}_l\left(f_{\mathrm{sx}}, f_{\mathrm{sy}}, f_{\mathrm{sz}}, \bar{f}_{\mathrm{d}}\right)$.

Step 3: Nonstationary Clutter Compensation:

From the distribution characteristics of clutter trajectory and power spectrum in Section 3, it can be seen that the clutter distribution of conformal array airborne radar varies with range, and the change is more obvious at short range. According to this feature, the method in this section only compensates the short-range clutter to the long-range reference point, and long-range clutter remains unchanged. Then, the whole clutter changes relatively smoothly with range cell. The compensation operation is as (25), shown at the bottom of the page, where $N^{(\mathrm{s})}K^{(\mathrm{s})}$ is the space-time smoothed subaperture product. $(f_{\mathrm{sx},i,0}, f_{\mathrm{sy},i,0}, f_{\mathrm{sz},i,0}, \bar{f}_{\mathrm{d},i,0})$ is the four-dimensional grid corresponding to the farthest unambiguous range cell, that is, the position of the reference point. S_1 is the range cell set corresponding to the short-range nonstationary clutter, S_2 is the range cell set of the long-range stationary clutter, and N_I is the number of grids divided in a single range ring.

In the process of nonstationary clutter compensation, the relationship between the compensated clutter patch and the reference clutter patch is that the azimuth angle is fixed and the pitch angle changes. The range of pitch angle between 0° and 8° is generally regarded as the stationary zone, and the range between 8° and 90° is the nonstationary zone.

Step 4: Clutter Covariance Matrix Estimation:

The clutter signal is approximately stationary distribution by means of step 3, and the estimated clutter covariance matrix is

$$\hat{\boldsymbol{R}}_l = \frac{1}{L}\sum_{l=1}^{L} \widehat{\boldsymbol{X}}_l\widehat{\boldsymbol{X}}_l^{\mathrm{H}} \tag{26}$$

where L is the number of compensated training samples.

Step 5: Space-Time Adaptive Processing:

The space-time adaptive weight of the kth Doppler channel and the lth range cell is

$$\boldsymbol{W}_{l,k} = \mu\hat{\boldsymbol{R}}_l^{-1}\boldsymbol{S}(f_{\mathrm{s}0}, \bar{f}_{\mathrm{d},k}) \tag{27}$$

where μ is a constant, $\boldsymbol{S}(f_{\mathrm{s}0}, \bar{f}_{\mathrm{d},k})$ is the space-time steering vector of conformal array, $f_{\mathrm{s}0}$ is the desired spatial frequency, and $\bar{f}_{\mathrm{d},k}$ is the normalized Doppler frequency to be detected.

$$\widehat{\boldsymbol{X}}_l = \frac{NK}{N^{(\mathrm{s})}K^{(\mathrm{s})}}\left(\begin{array}{l} \displaystyle\sum_{l\in S_1}\sum_{i=1}^{N_I}\sqrt{\tilde{\hat{\boldsymbol{P}}}_l\left(f_{\mathrm{sx},i}, f_{\mathrm{sy},i}, f_{\mathrm{sz},i}, \bar{f}_{\mathrm{d},i}\right)}\boldsymbol{S}(f_{\mathrm{sx},i,0}, f_{\mathrm{sy},i,0}, f_{\mathrm{sz},i,0}, \bar{f}_{\mathrm{d},i,0}) \\ \displaystyle+\sum_{l\in S_2}\sum_{i=1}^{N_I}\sqrt{\tilde{\hat{\boldsymbol{P}}}_l\left(f_{\mathrm{sx},i}, f_{\mathrm{sy},i}, f_{\mathrm{sz},i}, \bar{f}_{\mathrm{d},i}\right)}\boldsymbol{S}(f_{\mathrm{sx},i,l}, f_{\mathrm{sy},i,l}, f_{\mathrm{sz},i,l}, \bar{f}_{\mathrm{d},i,l}) \end{array}\right) \tag{25}$$

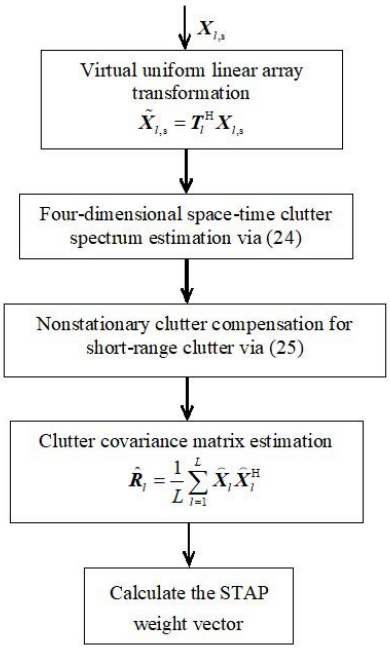

FIGURE 9. The flow chart of 4D-STC method.

In summary, the implementation steps of the proposed 4D-STC method are showed in Fig. 9.

B. COMPARISON WITH OTHER METHODS

The clutter reconstruction methods in [22]–[24] need the flight parameters and position information of the platform system as a priori knowledge to obtain the space time steering vectors of clutter patches, and use the clutter spectrum to reconstruct the clutter covariance matrix. Therefore, the robustness of these methods is poor when the prior parameter error or array error exist. In [21], the RBC-RA method compensates the unambiguous range cell and the ambiguous range cell to the corresponding reference range cell, and reconstructs the clutter covariance matrix of the reference range cell. The non-stationary clutter compensation accuracy is high, but it is strongly dependent on the airborne radar system parameters and has the problem of target signal movement.

Compared with the traditional clutter construction method, the proposed method realizes the effective estimation of clutter power through space-time smoothing, and eliminates the influence of system parameter error on the performance of the proposed method.

In the traditional methods, only the clutter signal of the unambiguous range cell corresponding to the cell to be detected is usually compensated. In contrast, all short-range cells of non-stationary clutter are compensated in the proposed method, and the compensated reference cell is fixed to the farthest unambiguous range cell. The advantages of the proposed 4D-STC method are as follows: (1) The accurate position of the clutter trajectory is not required. (2) It effectively solves the influence of the spectrum broadening caused by space-time error. Besides, because the target signal and clutter signal are not in the same plane in the four-dimensional space-time domain, the method does not cause the target signal movement.

TABLE 1. Parameters of simulation experiments.

Parameter	Symbol	Value
Platform height	h	8km
Platform velocity	V_R	140m/s
Number of elements in elevation	M	12
Number of elements in elevation	M	12
Number of elements in azimuth	N	12
Number of range ambiguities	N_r	5
PRF	f_r	2434.8Hz
Radar wavelength	λ	0.23m
Signal bandwidth	B	5MHz
Number of training samples	L	384
Number of pulses	K	16

V. EXPERIMENTAL RESULTS

This section takes the nose cone conformal array and cylindrical array as examples to analyze the effectiveness of the adaptive compensation method based on the four-dimensional space-time clutter spectrum. The simulation parameters are given in Table 1. And we compare the performance of the sample matrix inversion (SMI) method [6], the RBC-RA method [21] and the proposed 4D-STC method. It should be noted that since the nose cone conformal array and cylindrical array simulated in this section can only sense the spatial frequencies in the X-axis and Y-axis directions, the experiments in this section only analyze clutter power spectrum estimation and compensation from the viewpoint of space-time three-dimension.

A. EXPERIMENT 1: CLUTTER POWER SPECTRUM ESTIMATION PERFORMANCE

Figs. 10 and 11 show the estimated clutter power spectra and true clutter power spectra of the nose cone conformal array and cylindrical array airborne radar at range cell 500, respectively. It can be seen that the clutter power spectrum estimated by the virtual linear array transformation and space-time smoothing processing is basically consistent with the true spectrum. The clutter power estimated for the cylindrical array is relatively high, and it is caused by the pseudo-inverse operation corresponding to the non-matching angle in the process of transforming the cylindrical array into the virtual forward-looking linear array.

Note that the clutter power spectrum estimated for the cylindrical array without virtual ULA transformation occupies a larger portion of the space time plane as shown in Fig. 11(c), and it will lead to clutter power spectrum estimation error.

B. EXPERIMENT 2: NONSTATIONARY CLUTTER COMPENSATION PERFORMANCE

The performance of the four-dimensional compensation is shown in Figs. 12 and 13, where Figs. 12(a) and 13(a) show the clutter and target distribution before compensation at range cell 500 corresponding to the virtual uniform linear

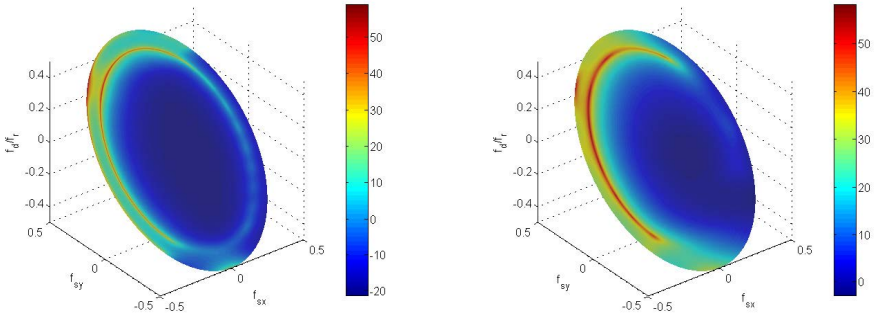

FIGURE 10. Clutter power spectrum estimation of nose cone conformal array. (a) True clutter power spectrum. (b) Estimated clutter power spectrum.

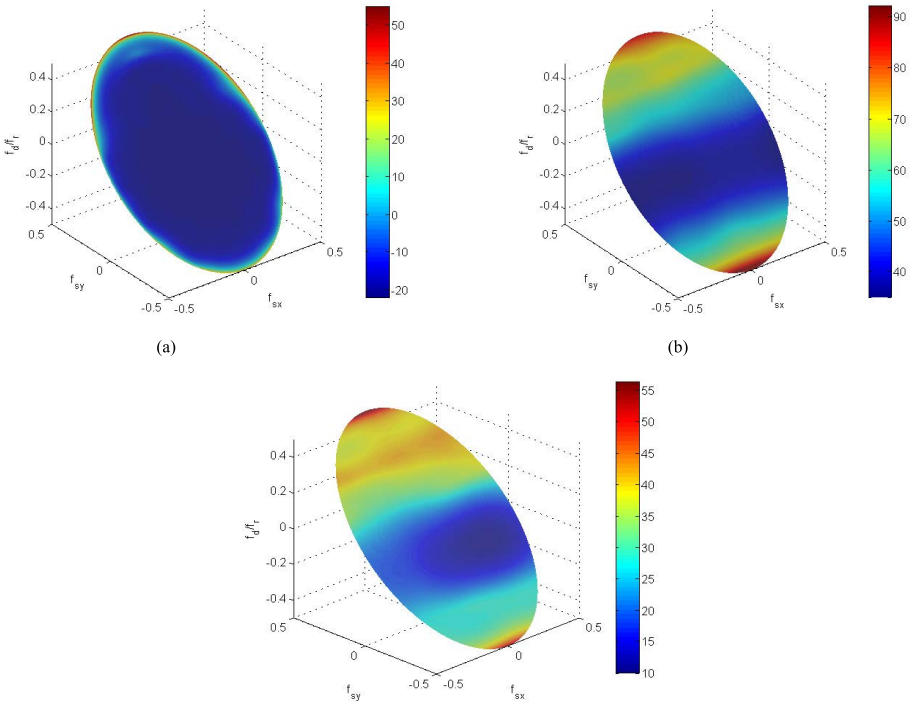

FIGURE 11. Clutter power spectrum estimation of cylindrical array. (a) True clutter power spectrum. (b) Estimated clutter power spectrum with virtual ULA transformation. (c) Estimated clutter power spectrum without virtual ULA transformation.

array, and Figs. 12(b) and 13(b) show the clutter power spectra corresponding to the conformal array estimated by using all the training samples after compensation. The asterisks indicate the location of moving target. There is only one case that the target locates within the clutter spectrum, that is, the target locates on the ground and the velocity of target is perpendicular to the line of sight from the radar. Fortunately, this case usually remains fleetling. Therefore, this case is not considered in the section. In the simulation, it is assumed that the coordinate of target in the $(f_{sx}, f_{sy}, \bar{f}_d)$ domain is $(-0.0244, 0.0812, -0.4)$.

The following conclusions are obtained from Figs. 12 and 13. (1) After four-dimensional compensation, the clutter power is concentrated at the farthest unambiguous range cell, and the influence of the short-range nonstationary clutter is basically eliminated. (2) Before compensation, the short-range nonstationary clutter is obvious, and the characteristic is consistent with the clutter power spectrum characteristic of the uniform linear array taking into account range ambiguity. (3) The target position remains unchanged during the clutter compensation process. The reason is that clutter and target can be separated in the four-dimensional space-time domain.

C. EXPERIMENT 3: SCNR LOSS

Figs. 14 and 15 show the signal-to-clutter-plus-noise ratio (SCNR) loss performance of the nose cone conformal array and cylindrical array airborne radar with or without

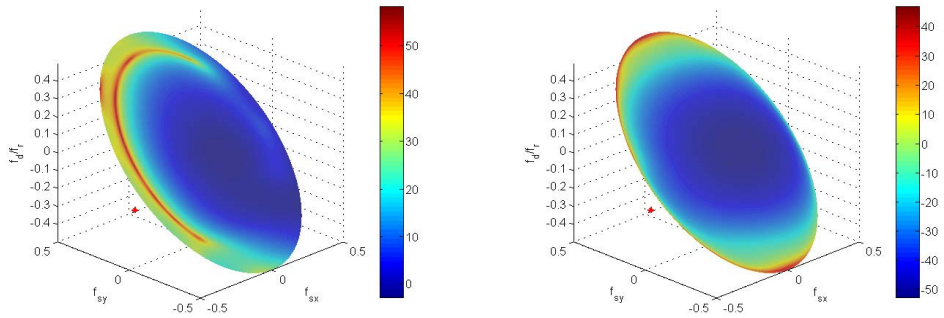

FIGURE 12. Clutter power spectrum of nose cone conformal array. (a) Before four-dimensional compensation. (b) After four-dimensional compensation.

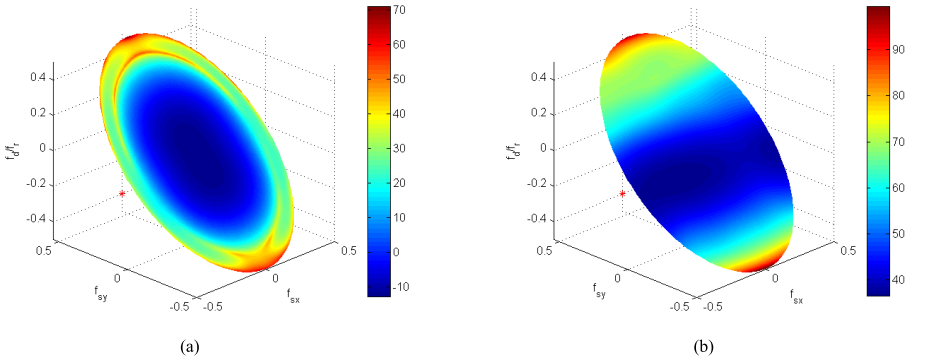

FIGURE 13. Clutter power spectrum of cylindrical array. (a) Before four-dimensional compensation. (b) After four-dimensional compensation.

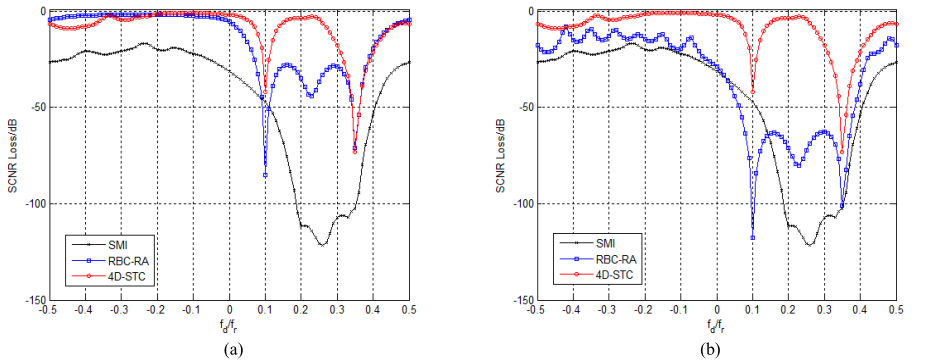

FIGURE 14. SCNR loss for nose cone conformal array. (a) Without prior parameter error. (b) With prior parameter error.

prior parameter error. The prior parameter refers to the flying height of the aircraft. The Gaussian distribution of the height error in the simulation is assumed to be N(2,1). The following conclusions are obtained from Figs. 14 and 15. (1) The 4D-STC method has the best performance, followed by the RBC-RA method. The SMI method does not perform any compensation, so the performance is the worst. (2) Whether there is prior parameter error or not, the 4D-STC method can effectively suppress clutter over the entire Doppler domain, and its two notches correspond to the front and back mainlobes after compensation respectively, as shown in Figs. 14(b) and 15(b). (3) The performance of the RBC-RA method is seriously affected by the prior parameter error. The reason is that the method compensates the range ambiguous clutter to the corresponding reference point position respectively, so it has a strong dependence on the height parameter of platform. The RBC-RA method has the two identical notches as the 4D-STC method, and there is an additional notch for the nose cone conformal array, which corresponds to the mainlobe clutter of the first unambiguous range cell in the short range, as shown in Fig. 14 (a). For the cylindrical array, there are two additional notches, corresponding to the

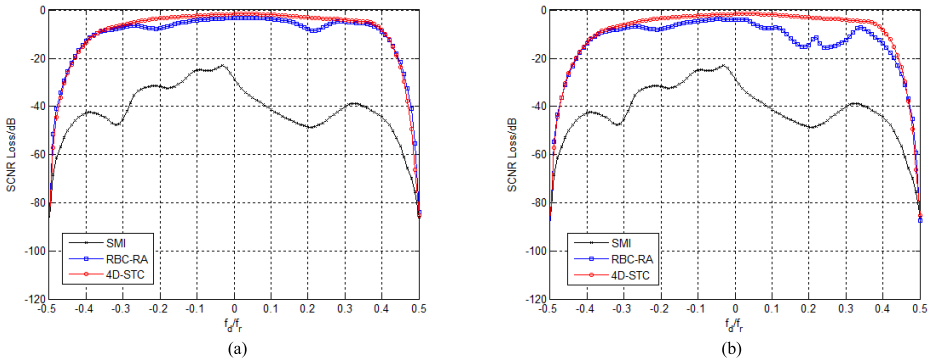

FIGURE 15. SCNR loss for cylindrical array. (a) Without prior parameter error. (b) With prior parameter error.

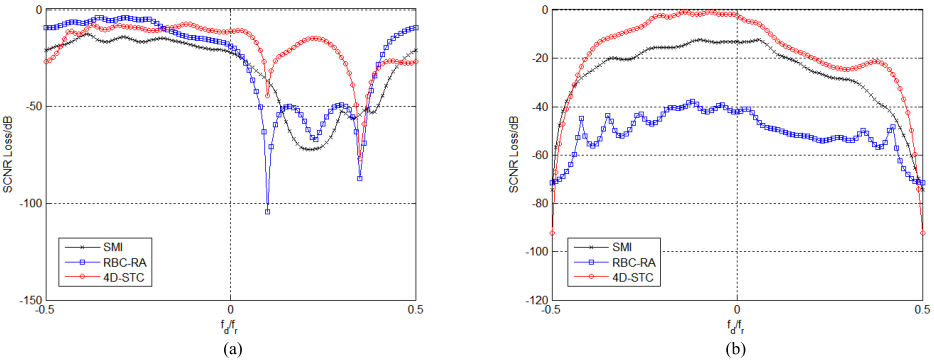

FIGURE 16. SCNR loss for conformal array with array errors. (a) Nose cone conformal array. (b) Cylindrical array.

front and back mainlobe clutter of the first unambiguous range cell, as shown in Fig. 15 (a). (4) Performance of the SMI method is the worst, especially in the wide notch. The reason is that a large number of nonstationary training samples are averaged to estimate clutter covariance matrix, and the clutter spectrum is broadened obviously.

To be general, except for prior parameter error, the array errors, such as array element position error, channel mismatch, and mutual coupling [7], [9], usually degrade the performance of the clutter suppression method. So we take above array errors into consideration. Assuming that the amplitude error follows Gaussian distribution, and the phase error follows uniform distribution, that is $\varepsilon_n \sim N\left(0, \xi^2\right), \phi_n \sim U\left(-\zeta, \zeta\right)$, among them, $\xi = 0.02$, $\zeta = 0.01$.

Fig. 16 shows the SCNR loss performance of conformal array with array error. We can obtain the following conclusions from Fig. 16. (1) In most clutter regions, the 4D-STC method has the best performance, followed by the RBC-RA method and the SMI method. (2) As for the conformal array, array errors may degrade the performance of the clutter suppression methods to some degree, especially for the RBC-RA method with cylindrical array. Relatively speaking, the proposed method has strong robustness to array errors.

VI. CONCLUSION

In this paper, we have established a clutter signal model of the conformal array airborne radar, and analyzed the clutter characteristics of the conformal array airborne radar in detail. Besides, a four-dimensional space-time clutter spectrum adaptive compensation method for conformal array airborne radar was proposed. The simulation results show that the proposed method compensates nonstationary clutter in the four-dimensional space-time domain, and it does not lead the target signal movement. What's more, the proposed method overcomes the influence of prior system parameter error and array error on compensation processing and has strong robustness under practical environments.

So for the future developments for this study, we can use the 4D-STC method to improve the suppression performance of severe nonstationary clutter environment faced by the bistatic (multistatic) airborne radar with special array like the conformal array or end-fire array. Then, the future work is how to solve the problem of simultaneous effective suppression of nonhomogeneous clutter and nonstationary clutter for conformal array airborne radar.

REFERENCES

[1] R. K. Hersey, "Adaptive detection and estimation using a conformal array antenna," M.S. thesis, Georgia Inst. Technol., Atlanta, GA, USA, 2004.

[2] A. De Maio, D. Orlando, C. Hao, and G. Foglia, "Adaptive detection of point-like targets in spectrally symmetric interference," *IEEE Trans. Signal Process.*, vol. 64, no. 12, pp. 3207–3220, Jun. 2016.

[3] G. Foglia, C. Hao, A. Farina, G. Giunta, D. Orlando, and C. Hou, "Adaptive detection of point-like targets in partially homogeneous clutter with symmetric spectrum," *IEEE Trans. Aerosp. Electron. Syst.*, vol. 53, no. 4, pp. 2110–2119, Aug. 2017.

[4] P. Addabbo, S. Han, D. Orlando, and G. Ricci, "Learning strategies for radar clutter classification," *IEEE Trans. Signal Process.*, vol. 69, pp. 1070–1082, 2021.
[5] D. Xu, P. Addabbo, C. Hao, J. Liu, D. Orlando, and A. Farina, "Adaptive strategies for clutter edge detection in radar," *Signal Process.*, vol. 186, Sep. 2021, Art. no. 108127.
[6] J. Ward, "Space-time adaptive processing for airborne radar," MIT Lincoln Lab., Lexington, MA, USA, Tech. Rep. 1015, 1994.
[7] R. Klemm, *Principles of Space-Time Adaptive Processing*, 3rd ed. London, U.K.: IEE Publishers, 2006.
[8] M. Barbary and P. Zong, "Novel anti-stealth on sub-Nyquist scattering wave deception jammer with stratospheric balloon-borne bistatic radar using KA-STAP-FTRAB algorithm," *IEEE Sensors J.*, vol. 15, no. 11, pp. 6437–6453, Nov. 2015.
[9] S. Zhu, G. Liao, J. Xu, L. Huang, and H. C. So, "Robust STAP based on magnitude and phase constrained iterative optimization," *IEEE Sensors J.*, vol. 19, no. 19, pp. 8650–8656, Oct. 2019.
[10] M. Zatman, "Circular array STAP," *IEEE Trans. Aerosp. Electron. Syst.*, vol. 36, no. 2, pp. 510–517, Apr. 2000.
[11] M. Zatman, "The properties of adaptive algorithms with time varying weights," in *Proc. IEEE Sensor Array Multichannel Signal Process. Workshop. SAM*, Cambridge, MA, USA, Mar. 2000, pp. 82–86.
[12] S. D. Hayward, "Adaptive beamforming for rapidly moving arrays," in *Proc. Int. Radar Conf.*, Beijing, China, Oct. 1996, pp. 480–483.
[13] G. K. Borsari, "Mitigating effects on STAP processing caused by an inclined array," in *Proc. IEEE Radar Conf. Challenges Radar Syst. Solutions*, Dallas, TX, USA, May 1998, pp. 135–139.
[14] O. Kreyenkamp and R. Klemm, "Doppler compensation in forward-looking STAP radar," *IEE Proc. Radar, Sonar Navigat.*, vol. 148, no. 5, pp. 253–258, Oct. 2001.
[15] F. Pearson and G. Borsari, "Simulation and analysis of adaptive interference suppression for bistatic surveillance radars," in *Proc. Adapt. Sensor Array Process. Workshop*, Lexington, MA, USA, Mar. 2001, pp. 1–21.
[16] K. P. Ong and B. Mulgrew, "Doppler compensation for JDL for airborne bistatic radar," in *Proc. IEEE Sensor Array Multichannel Signal Process. Workshop*, Cambridge, MA, USA, Aug. 2002, pp. 82–86.
[17] B. Himed, Y. Zhang, and A. Hajjari, "STAP with angle-Doppler compensation for bistatic airborne radars," in *Proc. IEEE Radar Conf.*, Long Beach, CA, USA, Apr. 2002, pp. 186–190.
[18] W. Melvin and M. Davis, "Adaptive cancellation method for geometry-induced nonstationary bistatic clutter environments," *IEEE Trans. Aerosp. Electron. Syst.*, vol. 43, no. 2, pp. 651–672, Apr. 2007.
[19] P. Ries, F. D. Lapierre, and J. G. Verly, "Geometry-induced range-dependence compensation for bistatic STAP with conformal arrays," *IEEE Trans. Aerosp. Electron. Syst.*, vol. 47, no. 1, pp. 275–294, Jan. 2011.
[20] Y. Xiong and W. Xie, "Non-stationary clutter suppression method for bistatic airborne radar based on adaptive segmentation and space–time compensation," *IET Radar, Sonar Navigat.*, vol. 15, no. 9, pp. 1001–1015, Sep. 2021.
[21] P. Ries, F. D. Lapierre, and J. G. VERLY, "Handling range-ambiguities in registration-based range-dependence compensation for conformal array STAP," in *Proc. IEEE Int. Radar Conf.*, Bordeaux, France, Oct. 2009, pp. 1–6.
[22] W. Xie, K. Duan, F. Gao, Y. Wang, and Z. Zhang, "Clutter suppression for airborne phased radar with conformal arrays by least squares estimation," *Signal Process.*, vol. 91, no. 7, pp. 1665–1669, 2011.
[23] M. Liu, L. Zou, X. Yu, Y. Zhou, X. Wang, and B. Tang, "Knowledge aided covariance matrix estimation via Gaussian kernel function for airborne SR-STAP," *IEEE Access*, vol. 8, pp. 5970–5978, 2020.
[24] Z. Li, Y. Zhang, H. Liu, B. Xue, and Y. Liu, "A robust STAP method for airborne radar based on clutter covariance matrix reconstruction and steering vector estimation," *Digit. Signal Process.*, vol. 78, pp. 82–91, Jul. 2018.
[25] J. R. Guerci and E. J. Baranoski, "Knowledge-aided adaptive radar at DARPA: An overview," *IEEE Signal Process. Mag.*, vol. 23, no. 1, pp. 41–50, Jan. 2006.
[26] G. T. Capraro, A. Farina, H. Griffiths, and M. C. Wicks, "Knowledge-based radar signal and data processing: A tutorial review," *IEEE Signal Process. Mag.*, vol. 23, no. 1, pp. 18–29, Jan. 2006.
[27] C. T. Capraro, G. T. Capraro, I. Bradaric, D. D. Weiner, M. C. Wicks, and W. J. Baldygo, "Implementing digital terrain data in knowledge-aided space-time adaptive processing," *IEEE Trans. Aerosp. Electron. Syst.*, vol. 42, no. 3, pp. 1080–1099, Jul. 2006.
[28] C. Hao, D. Orlando, G. Foglia, and G. Giunta, "Knowledge-based adaptive detection: Joint exploitation of clutter and system symmetry properties," *IEEE Signal Process. Lett.*, vol. 23, no. 10, pp. 1489–1493, Oct. 2016.
[29] W. Xie and Y. Wang, "STAP for airborne radar with cylindrical phased array antennas," *Signal Process.*, vol. 89, no. 5, pp. 883–893, May 2009.
[30] P. Ries, X. Neyt, F. D. Lapierre, and J. G. Verly, "Fundamentals of spatial and Doppler frequencies in radar STAP," *IEEE Trans. Aerosp. Electron. Syst.*, vol. 44, no. 3, pp. 1118–1134, Oct. 2008.
[31] S. U. Pillai, Y. L. Lim, and J. R. Guerci, "Generalized forward/backward subaperture smoothing techniques for sample starved STAP," *IEEE Trans. Signal Process.*, vol. 48, no. 12, pp. 3569–3574, Dec. 2000.
[32] R. K. Hersey, W. L. Melvin, J. H. Mcclellan, and E. Culpepper, "Adaptive ground clutter suppression for conformal array radar systems," *IET Radar, Sonar Navigat.*, vol. 3, no. 4, pp. 357–372, Aug. 2009.

YUANYI XIONG was born in Hubei, China, in 1990. He received the B.S. and M.S. degrees from the Wuhan University of Technology, Wuhan, China, in 2013 and 2016, respectively. He is currently pursuing the Ph.D. degree in information and communication engineering.

He is also a Lecturer with the Wuhan Radar Academy. His research interests include space-time adaptive processing, array signal processing, and airborne radar signal processing.

WENCHONG XIE (Member, IEEE) was born in Shanxi, China, in 1978. He received the Ph.D. degree in signal and information processing from the National University of Defense Technology, Changsha, China, in 2006.

He is currently a Professor with the Wuhan Radar Academy. His research interests include space-time adaptive processing, airborne radar signal processing, and airborne radar target detection.

YONGLIANG WANG was born in Zhejiang, China, in 1965. He received the Ph.D. degree from Xidian University, Xi'an, China, in 1994.

He is currently a Professor with the Wuhan Radar Academy. He is also a member of the Chinese Academy of Sciences. His research interests include space-time adaptive processing, radar signal processing, and array signal processing.